

Direct Synthesis of Long Single-Walled Carbon Nanotube Strands

H. W. Zhu,¹ C. L. Xu,¹ D. H. Wu,^{1*} B. Q. Wei,² R. Vajtai,²
P. M. Ajayan^{2*}

In the processes that are used to produce single-walled nanotubes (electric arc, laser ablation, and chemical vapor deposition), the typical lengths of tangled nanotube bundles reach several tens of micrometers. We report that long nanotube strands, up to several centimeters in length, consisting of aligned single-walled nanotubes can be synthesized by the catalytic pyrolysis of *n*-hexane with an enhanced vertical floating technique. The long strands of nanotubes assemble continuously from arrays of nanotubes, which are intrinsically long.

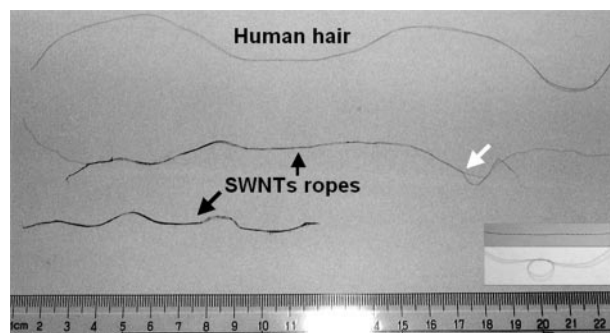
There has been much interest in the production and processing of carbon nanotubes since their discovery (1). Aligned multiwalled carbon nanotubes with a length of 2 mm (2), long single-walled nanotube (SWNT) ropes crossing microscopic lengths (3), and macroscopic SWNT fibers and ribbons (4) made by postprocessing techniques have been reported. For some applications, the mechanical and electrical properties of nanotubes can only be harnessed if long continuous nanotubes can be synthesized; for example, such structures may be used as strong, highly conducting microcables or as mechanically robust electrochemical microactuators. However, the creation of such continuous macroscopic strands of nanotubes during production still remains a challenge. We report the direct synthesis of long strands of ordered single-walled carbon nanotubes by an optimized catalytic chemical vapor deposition technique with a floating catalyst method in a vertical furnace (5), where *n*-hexane is catalytically pyrolyzed. The *n*-hexane solution with a given composition of ferrocene (0.018 g ml⁻¹) and thiophene (sulfur additive, 0.4 weight %) was introduced into the reactor at a rate of 0.5 ml min⁻¹ after heating the reactor to the pyrolysis temperature (1423 K), with hydrogen as the carrier gas flowing at a rate of 250 ml min⁻¹. SWNTs formed in abundance during this continuous process, and we obtained yields of ~0.5 g hour⁻¹. The formation of very long SWNT strands, also in large yields, is the unique characteristic of our vertical floating process.

The salient feature of our synthesis method is in the use of *n*-hexane in combination

with thiophene and hydrogen. Typically, ferrocene-assisted chemical vapor deposition of hydrocarbons (benzene, xylene) produces multiwalled carbon nanotubes at lower temperatures (~1050 K) and a mixture of single- and multiwalled nanotubes at higher temperatures (>1300 K) (6–8). The use of thiophene has been shown to increase the yield of SWNTs (8). The temperature and the hydrogen flow rates (which also have a positive influence in SWNT yield) are optimized in our technique to create a continuous process (9) in which large portions of long SWNTs are formed and assembled into macroscopic strands. Without hydrogen flow, the yield of nanotube growth rapidly decreases, and no long strands are produced. Replacing *n*-hexane with other hydrocarbons results in lower yields of SWNTs, and no large self-assembled strands are created. The strands contain impurities (~5 weight %), consisting of catalyst (Fe) particles and amorphous carbon, as determined from thermogravimetric analysis. Most of the catalyst particles can be removed by high-temperature vacuum annealing or refluxing the strands in nitric acid for several minutes.

Two samples of as-grown SWNT strands with lengths of 20 and 10 cm are shown in Fig. 1. These strands generally have a diameter of ~0.3 mm, which is larger than a

Fig. 1. Optical image showing a human hair and two as-grown SWNT strands (indicated by black arrows). The SWNT strands, with lengths of 20 and 10 cm, generally consist of thinner ropes (as indicated by the white arrow) and have a diameter of the order of 0.3 to 0.5 mm. The inset shows one straightened strand and another tied in a knot, demonstrating the high flexibility of the nanotube strand.



human hair. The edges of the SWNT strands are smooth and continuous, with a few individual nanotube bundles protruding out of the edge (Fig. 2A). The high-resolution view along a single rope indicates that it consists of well-aligned bundles of SWNTs (Fig. 2B). High-resolution transmission electron microscopy (HRTEM) images (Fig. 2C) show that each bundle is composed of aligned SWNTs. Raman spectroscopy measurements suggest that both metallic [characteristic Raman peaks around 197.4 cm⁻¹ (9,9) and 215.6 cm⁻¹ (11,5)] and semiconducting [around 146.6 cm⁻¹ (21,1)] SWNTs coexist with a wide distribution of diameters, ranging from 1.1 to 1.7 nm. However, a sharp Raman peak at 215.6 cm⁻¹ suggests that there is a dominant diameter of 1.1 nm for the nanotubes in the sample. We performed x-ray diffraction studies on the strands, focusing on the low-*Q* regions (scattering vector $Q = 4\pi\sin\theta/\lambda$), and we obtained the well-defined peak at $Q = 0.51 \text{ \AA}^{-1}$, corresponding to *d* (1,0) spacing of the nanotube triangular lattice (10, 11). The lattice parameter calculated from this peak position is 1.42 nm, which comes from a lattice assembled from 1.1-nm-diameter nanotubes; our data fit very well with calculated results of lattice parameters of finite crystallites made from nanotubes of different diameters (12).

We measured the macroscopic electrical resistivity on some of the long SWNT strands (with diameters from 50 μm to 0.5 mm) from room temperature to 5 K, using a four-probe method. The crossover temperature (from metallic to semiconducting) in the measured samples occurred at ~90 K. Metallic behavior was seen with resistivity $\rho = 5 \times 10^{-6}$ to 7×10^{-6} ohm·m between the temperature range of 90 to 300 K. This resistivity is about six times the value of a previously reported single bundle (13) but less than that of the as-grown and pressed materials. The temperature (90 K) at which the electrical behavior of the strands shifts from metallic to semiconducting differs from the previously reported value of 35 K (13). This is presumably because the relative amounts of metallic to semiconducting nanotubes (as well as the diameter distribution and packing) in our

¹Department of Mechanical Engineering, Tsinghua University, Beijing 100084, China. ²Department of Materials Science and Engineering, Rensselaer Polytechnic Institute, Troy, NY 12180, USA.

*To whom correspondence should be addressed. E-mail: wdh-dme@tsinghua.edu.cn, ajayan@rpi.edu

REPORTS

long nanotube strands is different compared to nanotube samples prepared by other techniques. However, the values of resistivity measured between probes are low enough to suggest that there are macroscopic lengths of continuous conducting paths (nanotubes) in the strands.

Because the nanotube strands are of macroscopic lengths and can be manipulated quite easily, direct tensile tests can be performed on individual strands. The stress in the strands depends on the actual cross section supporting the load, which is difficult to determine at any instant. An additional challenge in interpreting the test results is that a sizable contribution to strain could result from the slippage between parallel ropes or individual nanotubes in the ropes, depending on how the sample is gripped and loaded. We recorded direct tensile test measurements on individual SWNT strands of centimeter lengths, and these provided lower bound estimates for the mechanical properties (for example, the modulus) of the strands and suggest the robustness of these macroscopically long nanotube assemblies.

All samples used in tensile tests were as-grown strands of nanotubes, several centimeters in length. The strands were first separated with tweezers into several smaller strands having diameters from ~ 5 to ~ 20 μm . The starting diameter of the nanotube strand was easily measured with scanning electron microscopy (SEM) (Fig. 3A). These strands were then glued with silver paste onto two pieces of hard paper, which were then mounted in a tensile test machine (United SSTM-1-PC; United Calibration Corp., Huntington Beach, CA), where the loads could range from 0.001 to 200 N. During loading to failure, the nanotube strands, and hence the individual nanotubes, experience two different strains, elastic strain and plastic strain, owing to slippage between aligned nanotubes and real plastic deformation of individual nanotubes. This is consistent with the stress-strain curve shown in Fig. 4, which indicates that slippage and plastic deformation occurred before failure (14). Considering the possible variation in the strand diameter during the deformation process, as well as the difficulty in determining the changes in di-

ameter of the strands as deformation occurs, we plotted the true stress (σ_T) versus true strain (ϵ_T) curve (Fig. 4), rather than the usual engineering stress and strain; the true stress can be evaluated by knowing the strain at each point of loading (15). The true stress versus true strain and the load versus engineering strain curves have almost the same slopes in the elastic region of the curves (low strains). Young's modulus can be estimated from the linear part of the stress-strain curve at the low-strain regime [$<2\%$ (Fig. 4)], with observed values ranging from 49 to 77 GPa. This is about five times the modulus reported for oriented SWNT fibers and ribbons (4) and 50 times that of high-quality bucky paper (16).

These very long nanotube strands are handled and manipulated easily (see Fig. 1, inset, where the strand is tied into a knot), suggesting that these strands are not as brittle as nanotube aggregates prepared by other techniques. The Young's modulus estimates for these structures from the direct tensile tests fall short of values expected for individual nanotubes (17, 18) or small nanotube bundles (19, 20); however, the numbers we obtained for the modulus are lower bound estimates attributable to the uncertainty in knowing the exact cross-sectional area of the strands, supporting load. The nanotube strands are not monolithic structures and consist of parallel nanotube ropes separated by interstitial space. From our SEM measurements, we estimated the approximate volume fraction of nanotubes in the strands by analyzing the spacing between the nanotube ropes in the strands and found that this volume fraction is $<48\%$ (21). If one considers only this cross-sectional area supporting the load during the tensile test, the modulus values for the strands would increase from the above reported range (49 to 77 GPa) to a range of ~ 100

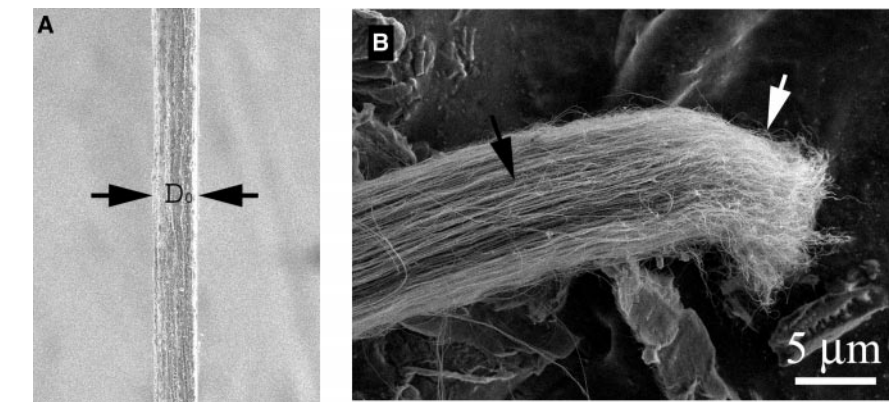
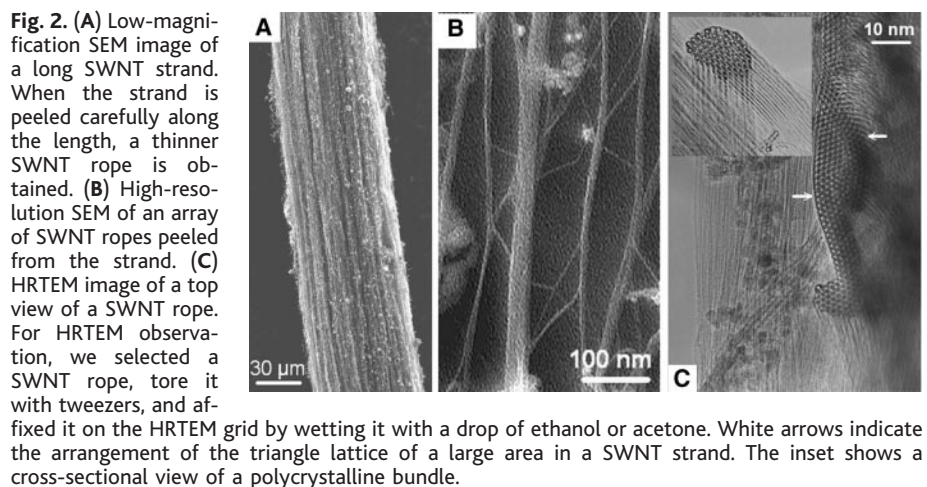


Fig. 3. Tensile test samples were prepared by separating a large nanotube strand into several small strands, which have the same length as the large original one. (A) The diameter D_0 of the small strand (~ 10 μm between the black arrows) was measured with SEM before the tensile test. The sample was observed again after measurements. (B) SEM image of a typical example of a broken nanotube strand after a tensile test. The broken part of the strand shows local deformation (white arrow), but not much pullout is observed [as compared with other parts of the strand (black arrow)].

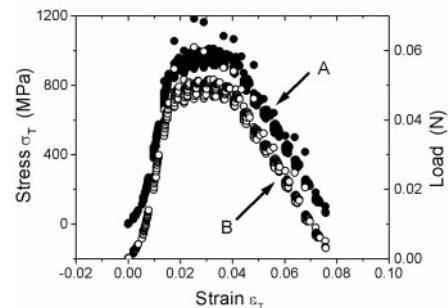


Fig. 4. (A) The true stress versus true strain curve (solid circles) and (B) the load versus engineering strain curve (open circles) for a nanotube strand during direct tensile testing. The true stress versus true strain curve has almost the same slope as that of the load versus engineering strain curve in the elastic strain regime. Young's modulus of the tested strand, as derived from the stress-strain curve, is ~ 77 GPa.

to ~150 GPa, consistent with the modulus values of large SWNT bundles (22). Although an individual SWNT has an elastic modulus of ~1 TPa, the value can decrease to ~100 GPa for nanotube bundles, owing to the internanotube defects (for example, imperfect lattice of nanotube bundles owing to different nanotube diameters) present along the bundles.

The long nanotube strands created by our direct synthesis technique are an alternative to the fibers and filaments spun from nanotube slurries (4). The mechanical and electrical properties of these strands are superior to the latter fibers: The strands can be produced in high yield and continuously, and the thickness of the strands and their length may be further optimized by tuning the processing conditions to produce practically useful nanotube-based macroscale cables.

References and Notes

1. S. Iijima, *Nature* **354**, 56 (1991).
2. Z. Pan et al., *Nature* **394**, 631 (1998).
3. H. M. Cheng et al., *Chem. Phys. Lett.* **289**, 602 (1998).
4. B. Vigolo et al., *Science* **290**, 1331 (2000).
5. L. J. Ci et al., *Carbon* **38**, 1933 (2000).
6. M. Endo et al., *J. Phys. Chem. Solids* **54**, 1841 (1993).
7. R. Andrews et al., *Chem. Phys. Lett.* **303**, 467 (1999).
8. H. M. Cheng et al., *Appl. Phys. Lett.* **72**, 3282 (1998).
9. Thiophene and ferrocene were dissolved in the carbon source (liquid *n*-hexane), sprayed into the hydrogen stream, and fed from the top of a vertical heated furnace. The hydrogen flow rate was then adjusted to provide the optimum conditions for nanotube strand formation. The gas flow carried the strands downstream, and the nanotube strands were collected at the bottom of the furnace.
10. A. Thess et al., *Science* **273**, 483 (1996).
11. P. Launois et al., *J. Nanosci. Nanotechnol.* **1**, 125 (2001).
12. Our data correspond to the larger tube numbers in the bundle ($N = 37$; $N = 91$), as displayed in figure 4 of S. Rols, R. Almairac, L. Henrard, E. Anglaret, J. L. Sauvageol [*Eur. Phys. J. B* **10**, 263 (1999)].
13. J. E. Fischer et al., *Phys. Rev. B* **55**, R4921 (1997).
14. P. H. Zhang, P. E. Lammert, V. H. Crespi, *Phys. Rev. Lett.* **81**, 5346 (1998).
15. The true strain ϵ_T is defined as $\epsilon_T = \ln(L_f/L_0)$, where L_f is the real length of the sample and L_0 is the original length of the sample. The true strain could also be described as $\epsilon_T = 2 \ln(D_0/D_f)$, assuming that the sample volume is constant, where D_0 and D_f are the original diameter and the real diameter of the sample during the measurement, respectively. Therefore, the true stress can be described as $\sigma_T = P/A = 4P \exp(\epsilon_T)/\pi D_0^2$, where P is the load and A is the real surface area supporting the load. Because $\ln(1+\epsilon) \approx \epsilon$ when $\epsilon < 0.1$, the true stress versus true strain curve has almost the same slope as that of the load versus engineering strain curve in the elastic strain regime.
16. R. H. Baughman et al., *Science* **284**, 1340 (1999).
17. M. M. J. Treacy, T. W. Ebbesen, J. M. Gibson, *Nature* **381**, 678 (1996).
18. E. W. Wong, P. E. Sheehan, C. M. Lieber, *Science* **277**, 1971 (1997).
19. M. F. Yu, B. S. Files, S. Arepalli, R. S. Ruoff, *Phys. Rev. Lett.* **84**, 5552 (2000).
20. J. P. Lu, *Phys. Rev. Lett.* **79**, 1297 (1997).
21. F. Li, H. M. Cheng, S. Bai, G. Gu, M. S. Dresselhaus, *Appl. Phys. Lett.* **77**, 3161 (2000).
22. L. Forró, C. Schöenberger, in *Carbon Nanotubes: Synthesis, Structure, Properties and Applications*, M. S. Dresselhaus, G. Dresselhaus, Ph. Avouris, Eds. (Springer, New York, 2001), pp. 329–390.
23. H.W.Z., C.L.X., and D.H.W. acknowledge financial support from the State Key Project for Fundamen-

tal Research of the Ministry of Science and Technology, China, under grant G2000264-04. P.M.A. acknowledges financial support from the NSF through a CAREER grant. B.Q.W. acknowledges support from the NSF Nanoscale Science and Engineering Center, at Rensselaer Polytechnic Insti-

tute, for the directed assembly of nanostructures. We also acknowledge useful discussions with N. Koratkar and technical assistance from D. Vanstele and Y. Choi.

10 October 2001; accepted 22 March 2002

Manipulating the Quantum State of an Electrical Circuit

D. Vion,* A. Aassime, A. Cottet, P. Joyez, H. Pothier, C. Urbina,† D. Esteve, M. H. Devoret‡

We have designed and operated a superconducting tunnel junction circuit that behaves as a two-level atom: the “quantrium.” An arbitrary evolution of its quantum state can be programmed with a series of microwave pulses, and a projective measurement of the state can be performed by a pulsed readout subcircuit. The measured quality factor of quantum coherence $Q_\varphi \cong 25,000$ is sufficiently high that a solid-state quantum processor based on this type of circuit can be envisioned.

Can we build machines that actively exploit the fundamental properties of quantum mechanics, such as the superposition principle or the existence of entangled states? Applications such as the transistor or the laser, often quoted as developments based on quantum mechanics, do not actually answer this question. Quantum mechanics enters into these devices only at the level of material properties, but their state variables such as voltages and currents remain classical. Proposals for true quantum machines emerged in the last decades of the 20th century and are now being actively explored: quantum computers (1), quantum cryptography communication systems (2), and detectors operating below the standard quantum limit (3). The major difficulty facing the engineer of a quantum machine is decoherence (4). If a degree of freedom needs to be manipulated externally, as in the writing of information, its quantum coherence usually becomes very fragile. Although schemes that actively fight decoherence have recently been proposed (5, 6), they need very coherent quantum systems to start with. The quality of coherence for a two-level system can be quantitatively described by the quality factor of quantum coherence $Q_\varphi = \pi\nu_{01}T_\varphi$, where ν_{01} is its transition frequency and T_φ is the coherence time of a superposition of the states. It is generally accepted that for active decoherence compensation mechanisms, Q_φ 's larger than $10^4 \nu_{01} t_{op}$ are nec-

essary, t_{op} being the duration of an elementary operation (7).

Among all the practical realizations of quantum machines, those involving integrated electrical circuits are particularly attractive. However, unlike the electric dipoles of isolated atoms or ions, the state variables of a circuit, like voltages and currents, usually undergo rapid quantum decoherence because they are strongly coupled to an environment with a large number of uncontrolled degrees of freedom (8). Nevertheless, superconducting tunnel junction circuits (9–13) have displayed Q_φ 's up to several hundred (14), and temporal coherent evolution of the quantum state has been observed on the nanosecond time scale (10, 15) in the case of the single Cooper pair box (16). We report here a new circuit built around the Cooper pair box with Q_φ in excess of 10^4 , whose main feature is the separation of the write and readout ports (17, 18). This circuit, which behaves as a tunable artificial atom, has been nicknamed a “quantrium.”

The basic Cooper pair box consists of a low-capacitance superconducting electrode, the “island,” connected to a superconducting reservoir by a Josephson tunnel junction with capacitance C_j and Josephson energy E_J . The junction is biased by a voltage source U in series with a gate capacitance C_g . In addition to E_J , the box has a second energy scale, the Cooper pair Coulomb energy $E_{CP} = (2e)^2/2(C_g + C_j)$. When the temperature T and the superconducting gap Δ satisfy $k_B T \ll \Delta/\ln N$ and $E_{CP} \ll \Delta$, where N is the total number of paired electrons in the island, the number of excess electrons is even (19, 20). The Hamiltonian of the box is then

$$\hat{H} = E_{CP}(\hat{N} - N_g)^2 - E_J \cos \hat{\theta} \quad (1)$$

where $N_g = C_g U/2e$ is the dimensionless gate

Quantronics Group, Service de Physique de l'Etat Condensé, Direction des Sciences de la Matière, Commissariat à l'Energie Atomique-Saclay, 91191 Gif-sur-Yvette, France.

*To whom correspondence should be addressed. E-mail: vion@drecam.saclay.cea.fr

†Member of CNRS.

‡Present address: Applied Physics Department, Yale University, New Haven, CT 06520, USA.